J Mater Sci (2017) 52:4521–4531

Facile preparation of ternary Ag_2CO_3/Ag/PANI composite nanorods with enhanced photoactivity and stability

Fang Chen[1], Yadan Wu[1], Jiqiang Ning[2], Jiabin Ren[1], Ziyang Zhang[2], Changcheng Zheng[3], Yijun Zhong[1,*], and Yong Hu[1,4,*]

[1] *Institute of Physical Chemistry, Zhejiang Normal University, Jinhua 321004, People's Republic of China*
[2] *Suzhou Institute of Nano-Tech and Nano-Bionics, Chinese Academy of Sciences, Suzhou 215123, People's Republic of China*
[3] *Department of Mathematical Sciences, Mathematics and Physics Centre, Xi'an Jiaotong-Liverpool University, Suzhou 215123, People's Republic of China*
[4] *State Key Lab of Silicon Materials, College of Materials Science and Engineering, Zhejiang University, Hangzhou 310027, People's Republic of China*

Received: 18 October 2016
Accepted: 16 December 2016
Published online: 6 January 2017

ABSTRACT

One-dimensional ternary nanostructures, Ag_2CO_3 nanorod cores coated with an intermediate layer of Ag nanoparticles (NPs) and a sheath of conducting polymer polyaniline (PANI), Ag_2CO_3/Ag/PANI composite nanorods (CNRs), were successfully prepared via a facile two-step method. Ag NPs were first uniformly anchored onto the Ag_2CO_3 nanorods to form binary Ag_2CO_3/Ag CNRs with an in situ visible-light-induced reduction strategy, and then the Ag_2CO_3/Ag CNRs were coated with PANI of different contents through a simple chemisorption approach. The as-obtained hybrids exhibit significantly enhanced photoelectrochemical current response and photoactivity in degrading methyl orange under visible-light illumination ($\lambda > 420$ nm). The improved photoactivity was found to be related to the intermediate Ag between Ag_2CO_3 and PANI which facilitates the separation efficiency of photogenerated carriers, and an optimal weight percent of 2.0% PANI was observed. The origin of enhanced photoactivity was further investigated by a radical-trapping test, and a Z-scheme mechanism was proposed to explain the charge separation behaviors.

Introduction

In recent years, hetero-nanostructured photocatalysts have been widely examined from both fundamental and practical perspectives such as in water treatments [1–5]. Fast recombination of photogenerated electron–hole pairs is the major cause of low utilization rate of solar light, and it is still a great challenge to obtain enhanced photocatalytic efficiency with currently available photocatalysts. Conducting polymers,

Address correspondence to E-mail: yjzhong@zjnu.edu.cn; yonghu@zjnu.edu.cn

DOI 10.1007/s10853-016-0697-7

including polypyrrole (PPy), polythiophene (PTP), polyaniline (PANI), and their derivatives, exhibit good environmental stability and electrical conductivity, a wide range of visible-light absorption, and fast charge carrier transfer ability, making them useful in the field of photocatalysis [6–10]. Being relatively cheap and easy to synthesize, PANI has been intensively studied as one of the most promising conducting polymers [11]. Various reports have demonstrated that semiconductor composite photocatalysts modified with PANI, such as PANI/CdS [12], PANI/TiO_2 [13], PANI/$BiVO_4$ [14], and PANI/ZnO [15], with a higher separation efficiency of photogenerated electron–hole pairs, exhibit greatly improved photocatalytic performance in photodegrading organic pollutants under visible-light irradiation.

Very recently, Ag-based compounds have been regarded as a new family of high-efficiency visible-light-driven photocatalytic materials [16–18], and especially one-dimensional (1D) Ag-based heterostructured photocatalysts have attracted extensive attention because of their high aspect ratios and novel physicochemical properties [19–21]. We have successfully synthesized 1D binary MS–Ag (M = Ag, Pb, Zn, Cd) hybrid nanotubes and Ag_2CO_3/Ag/AgBr ternary composite nanorods (CNRs) using Ag_2CO_3 NRs as the template, which all exhibit significantly enhanced visible-light-driven photoactivity for organic pollutant degradation [22–24]. However, some inherent limitations of Ag_2CO_3 material, such as incompatibility between various materials, usually result in poor structural stability and uniformity of the resulting nanocomposites. Therefore, it is of great interest to develop suitable surface engineering methods to synthesize Ag_2CO_3-based nanocomposites and to inhibit their photocorrosion damage. Coating Ag_2CO_3 NRs with a thin layer of PANI may be an effective method to stabilize the surface and inhibit the photocorrosion process. More importantly, the properties of the final product, such as optical and catalytic properties, might also be altered by the modification of PANI nanocoating.

In this work, we have designed another ternary hybrid photocatalytic structure, 1D Ag_2CO_3/Ag/PANI CNRs, and herein report the preparation method and improved photocatalytic performance. The Ag_2CO_3/Ag/PANI CNRs were prepared via a facile in situ visible-light-induced reduction of Ag_2CO_3 NRs followed by a simple chemisorption of PANI. As expected, the as-obtained 1D ternary Ag_2CO_3/Ag/PANI CNRs exhibited significantly enhanced photoelectrochemical current response and photoactivity for the photodegradation of methyl orange (MO) under visible-light illumination ($\lambda > 420$ nm), and an optimal PANI weight percent (2.0%) was observed. To understand the origin of the observed enhanced photoactivity, a radical-trapping test was also performed, and a Z-scheme charge transfer mechanism was proposed to describe the separation behaviors of photogenerated carriers. This work demonstrates the synthesis of a visible-light-responsive composite photocatalyst and its potential in environmental remediation applications.

Experimental section

The reagents utilized in this work, purchased from the Shanghai Chemical Reagent Factory, were all of analytical grade and used as received without further purification. The Ag_2CO_3/Ag/PANI CNRs were prepared via a two-step strategy, in which Ag_2CO_3/Ag CNRs were first obtained and then PANI was coated.

Synthesis of 1D binary Ag_2CO_3/Ag CNRs

To obtain Ag_2CO_3/Ag CNRs, Ag_2CO_3 NRs were first prepared by a simple precipitation process. Briefly, 0.5 mol of $AgNO_3$ and 1.0 g of polyvinylpyrrolidone (PVP) were dissolved in 20 mL of distilled water to obtain a clear solution, and 20 mL of pre-prepared $NaHCO_3$ aqueous solution (0.05 M) was then dropwise added. After several minutes of precipitation, the solution turned gray, indicating the formation of Ag_2CO_3 NRs. Then, the as-prepared Ag_2CO_3 NRs were collected by centrifugation, washed with distilled water and ethanol for several times, and dried at 60 °C for 6 h in a vacuum oven. The Ag_2CO_3 NRs were dispersed in water and irradiated with visible light ($\lambda > 420$ nm) for about 1 h to produce 1D binary Ag_2CO_3/Ag CNRs [24].

Synthesis of 1D ternary Ag_2CO_3/Ag/PANI CNRs

PANI was first prepared via a typical process [25], started with dispersing 10 mL of aniline in 200 mL of HCl (1 M) to form a hazel-colored transparent solution. 20 g of $(NH_4)S_2O_8$ was dissolved in 200 mL of 1 M HCl and then mixed with the hazel solution. The

mixture was stirred until a brown slurry was obtained and then kept at 0 °C for 5 h to allow the polymerization reaction to complete. The obtained suspension was centrifuged, washed several times with distilled water and ethanol, and then dissolved in 100 mL of 0.1 M $NH_3{\cdot}H_2O$ by stirring for 24 h to produce PANI. The resulting PANI was collected by centrifugation, washed with distilled water and ethanol for several times, and dried at 60 °C for 8 h in a vacuum oven. Finally, Ag_2CO_3/Ag/PANI hybrid photocatalysts were prepared by dispersing the as-prepared Ag_2CO_3/Ag binary CNRs and PANI in 20 mL of tetrahydrofuran (THF) and stirring for 12 h, and the collected products were washed with distilled water and ethanol three times before being dried at 60 °C for 8 h. To investigate the effect of PANI on the formation of 1D ternary Ag_2CO_3/Ag/PANI composite photocatalysts, 50 mg of Ag_2CO_3/Ag CNRs were mixed with different amounts of PANI to obtain a series of products with different weight percents of PANI, 0.5, 1.0, 2.0, 3.0, and 5.0%, which are denoted as samples CNR-0.5, CNR-1, CNR-2, CNR-3, and CNR-5, respectively.

Characterizations

Scanning electron microscopy (SEM) characterization was performed with a Hitachi S-4800 scanning electron micro-analyzer with an accelerating voltage of 15 kV, and powder X-ray diffraction (XRD) measurements were performed with a Philips PW3040/60 X-ray diffractometer using Cu Kα radiation at a scanning rate of 0.06 $^{\circ}\cdot s^{-1}$. A PerkinElmer Lambda 900 UV–Vis spectrophotometer was used to acquire absorption spectra at room temperature, and Fourier transform infrared (FT-IR) spectra were recorded on a Nicolet NEXUS 670 FT-IR spectrometer using KBr pellets. Transmission electron microscopy (TEM) and high-resolution transmission electron microscopy (HRTEM) were conducted using a JEM-2100F field emission TEM. Further evidence for the composition of the products was obtained from X-ray photoelectron spectroscopy (XPS) measurements using a Kratos Axis ULTRA X-ray photoelectron spectrometer with Al Kα X-ray as the excitation source. Electrochemical impedance spectroscopy (EIS) spectra were acquired by employing an AC voltage of 10 mV amplitude in the frequency range of 0.1 Hz to 100 kHz in a three-electrode system with a 5 mM $K_3[Fe(CN)_6]$ and 1 M KCl aqueous mixture.

Photocatalytic test

The photocatalytic activity of the Ag_2CO_3/Ag/PANI hybrid products was evaluated by the degradation of MO dyes (analytical grade) under visible-light illumination. The light source is a 500 W Xe lamp with a 420-nm cut-on filter. All experiments were conducted at room temperature in air. In a typical process, 10 mg of the as-prepared Ag_2CO_3/Ag/PANI sample was added into 20 mL of MO solution (concentration of 5 mg/L), dispersed in an ultrasonic bath for 5 min, and then stirred for 2 h in the dark to reach adsorption equilibrium between the catalyst and the solution. The mixture was then exposed to visible-light irradiation for photocatalytic test, and the suspension was removed by centrifugation at given time intervals before measuring the absorption spectra of MO using UV–Vis spectroscopy.

Radical-trapping experiment

In order to identify the major active species in the degrading MO, radical-trapping experiments were conducted using three chemicals, *i.e.*, benzoquinone (BQ, a superoxide anion radical scavenger, $O_2^{\cdot-}$), sodium bicarbonate ($NaHCO_3$, a hole scavenger), and isopropanol (IPA, an·OH radical scavenger) [26, 27]. Similar to photocatalytic test, 10 mg of the as-prepared samples, together with the scavengers, were added into 20 mL of MO solution (concentration of 5 mg/L), dispersed in an ultrasonic bath for 5 min, and stirred for 2 h in the dark to reach adsorption equilibrium. After being irradiated with visible light for given time intervals, the catalyst was removed by centrifugation and the absorption spectra of MO were measured using UV–Vis spectroscopy.

Photoelectrochemical characterization

The photoelectrochemical response was measured using a CHI840C electrochemical workstation with conventional three-electrode setup under visible-light illumination. The as-prepared sample paste was coated onto a slice of ITO glass with an area of $1 \times 1\ cm^2$ and then dried at room temperature, which was employed as the working electrode. A platinum wire and Ag/AgCl were used as the counter and reference electrodes, respectively, and a 0.02 M Na_2SO_4 aqueous solution was used as an electrolyte. A 500 W Xe lamp with a 420-nm cut-on filter was utilized as the visible-light source.

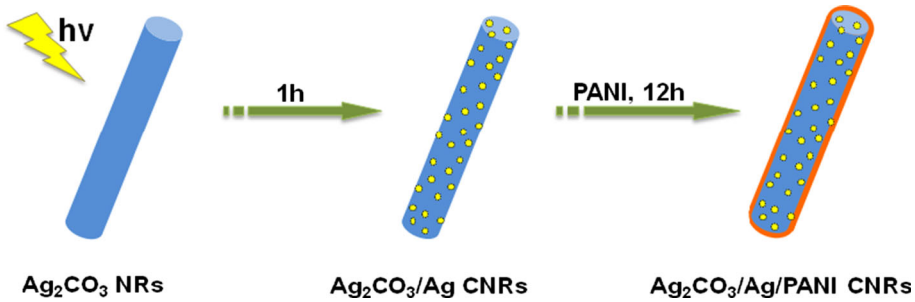

Scheme 1 Schematic illustration of the conversion processes from Ag_2CO_3 NRs to 1D ternary Ag_2CO_3/Ag/PANI CNRs.

Results and discussion

This simple two-step preparation strategy for the 1D ternary Ag_2CO_3/Ag/PANI CNRs is schematically depicted in Scheme 1. First, 1D binary Ag_2CO_3/Ag CNRs were prepared via a facile in situ visible-light-induced reduction of Ag_2CO_3 NRs, through which a conformal Ag NPs layer is uniformly deposited onto the Ag_2CO_3 NRs. Second, a simple chemisorption approach was used to obtain a series of PANI-modified Ag_2CO_3/Ag nanocomposites, i.e., ternary Ag_2CO_3/Ag/PANI CNRs. The crystallographic structure and phase purity of the as-prepared photocatalysts were first examined by XRD. The typical XRD patterns of the as-prepared pristine PANI, Ag_2CO_3 NRs, Ag_2CO_3/Ag CNRs, and CNR-2 are depicted in Fig. 1a. For the Ag_2CO_3/Ag CNRs and CNR-2, most of the diffraction peaks can be indexed as the hexagonal phase of Ag_2CO_3 (JCPDS No. 31-1236, $a = b = 9.180$ Å, $c = 6.485$ Å) and cubic Ag (JCPDS No. 04-0738, $a = b = c = 4.086$ Å). Nevertheless, some unindexed peaks are also observed, which may correspond to the monoclinic Ag_2CO_3 structure (JCPDS No. 26-0339 and 70-2184). The pristine PANI displays a broad peak at 2θ of approximately 20–25^0 [30], but no such diffraction peak can be observed in the sample CNR-2 because the loading amount is too small, suggesting that the modified PANI layer is very thin and well dispersed [28]. To reveal the existence of PANI layer at the surface of Ag_2CO_3/Ag CNRs, the FT-IR measurement on sample CNR-2 was further carried out. As displayed in Fig. 1b, the peaks at 1376, 1449, 881, and 704 cm^{-1} can be assigned to the stretching vibrations of carbonate, and the peaks at 1572 and 1490 cm^{-1} can be attributed to the C=C benzenoid rings and stretching of quinonoid, respectively [29, 30]. The characteristic peak around 1225 cm^{-1} represents the benzenoid C–N stretching vibration, while the peaks around 824 and 1158 cm^{-1} can be indexed to the C–H out-of-plane bending and in-plane bending modes, respectively [31, 32]. This result confirms that PANI was successfully coated onto the surface of Ag_2CO_3/Ag CNRs.

The morphology and structure of the as-prepared samples were characterized by SEM images. It can be observed from Fig. 1c that the as-prepared pristine PANI is completely composed of some irregular sheet-like agglomerates. The panoramic SEM images of the samples Ag_2CO_3 NRs, Ag_2CO_3/Ag CNRs, and CNR-2 are shown in Fig. 1d–f, revealing that all the samples are made up of well-defined nanorods with a nearly uniform size of ca. 200 nm in diameter and 1 μm in length. No pristine PANI morphology can be observed in the CNR-2 sample, indicating that PANI layer is coated onto the Ag_2CO_3/Ag CNRs. In addition, the SEM images of other samples with different contents of PANI are shown in Fig. 2, indicating that all the samples display the same rod morphology as CNR-2 and no obvious difference can be seen, except that the surface becomes slightly smooth as the content of PANI increases. The core–shell structure and the thicknesses of PANI layer of the as-prepared CNRs are further elucidated by TEM and HRTEM, as shown in Fig. 3. It can be clearly seen that all the samples display 1D nanostructures and obvious PANI shell layers. The thickness of PANI layer ranges from 1.0 to 8.0 nm with the increase of the PANI content (from 0.5 to 5.0%).

XPS spectra were examined to analyze the elemental composition and chemical states of the as-prepared sample CNR-2. As shown in Fig. 4a, the high-resolution spectrum of Ag 3d exhibits two individual peaks at 367.4 and 373.3 eV, corresponding to the binding energies of Ag $3d_{5/2}$ and $3d_{3/2}$, respectively. Especially, each peak can be resolved further into two peaks, indicating the presence of different chemical states: the peaks at 369.4 and 375.4 eV originate from Ag^0 [33], while the peaks at 367.4 and 373.3 eV are attributed to the Ag^+ species [34]. The high-resolution spectrum of N 1s is also

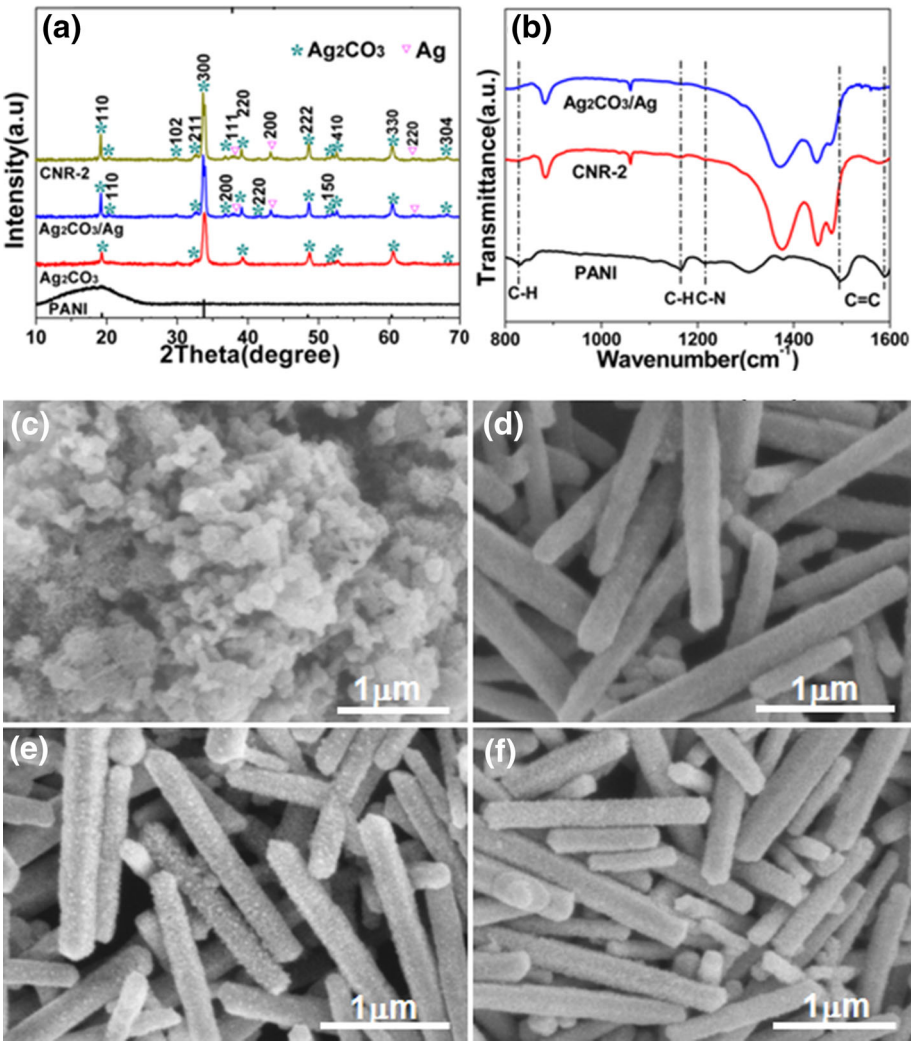

Figure 1 **a** XRD patterns of the as-prepared pristine PANI, Ag_2CO_3 NRs, Ag_2CO_3/Ag CNRs, and CNR-2, **b** FT-IR spectra of the as-prepared PANI, Ag_2CO_3/Ag CNRs, and CNR-2, and SEM images of the as-prepared **c** PANI, **d** Ag_2CO_3 NRs, **e** Ag_2CO_3/Ag CNRs, and **f** CNR-2.

displayed in Fig. 4b, with three peaks at 398.1, 399.1, and 400.8 eV, which can be attributed to the quinoid imine (–N=), benzenoid amine (–NH–), and cationic nitrogen ($–N^+–$) atoms, respectively, clearly confirming the existence of PANI in the product [35].

The photocatalytic activities of the as-prepared 1D ternary Ag_2CO_3/Ag/PANI CNRs were evaluated by photodegradation experiments of organic dye MO in an aqueous solution driven by visible-light irradiation ($\lambda > 420$ nm). Figure 5a presents the time profile of photodegradation using different samples, in terms of C/C_0, where C is the concentration of MO at a given illumination time and C_0 is the initial concentration of MO at dark adsorption equilibrium. It can be seen that, after 60 min of illumination, the degradation fractions for different photocatalysts are 21.9% (Ag_2CO_3/Ag binary CNRs), 25.1% (sample CNR-0.5), 45.5% (sample CNR-1), 71.9% (sample CNR-2), 52.2% (sample CNR-3), and 29.8% (sample CNR-5). The binary Ag_2CO_3/Ag CNRs exhibit the lowest degradation efficiency, and the photocatalytic activities of the as-prepared ternary CNRs are obviously enhanced. Meanwhile, it is noteworthy that the photocatalytic activity of the Ag_2CO_3/Ag/PANI CNRs does not improve monotonously with the increasing PANI content, and sample CNR-2 shows the best performance. Thus, there should be an optimal thickness of the PANI layer [36]. Specifically, the PANI polymer layer can enhance the adsorption capability of organic dyes, which can enrich the dye molecules on the surface of Ag_2CO_3, thus resulting in the acceleration of photocatalytic reactions. However, a thick and dense PANI layer (>2.0 wt%) may reduce the inherent optical absorption of Ag_2CO_3 and result in a rapid decrease in photogenerated charges, ultimately reducing the photocatalytic activity. In this

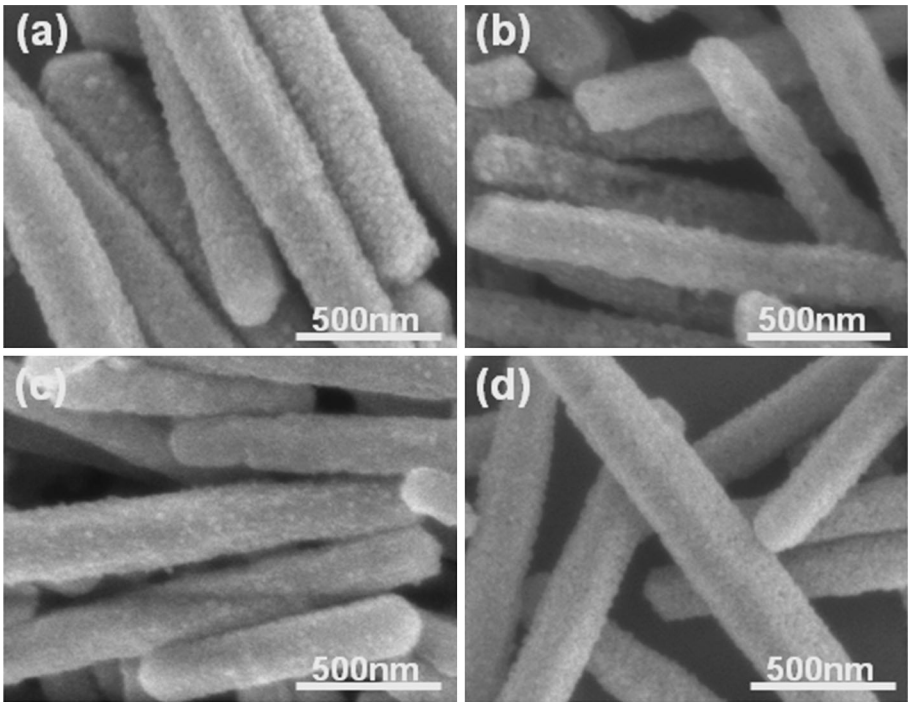

Figure 2 SEM images of the as-prepared 1D Ag_2CO_3/Ag/PANI ternary CNRs obtained with different weight percents of PANI: **a** CNR-0.5, **b** CNR-1, **c** CNR-3, and **d** CNR-5.

particular case, sample CNR-2 has the ideal PANI content that balances the effect of charge separation with carrier generation and results in the most favorable photoactivity. When the pollutant concentration is in the millimolar range, the photodegradation rate can generally be described by the Langmuir–Hinshelwood model in terms of pseudo first-order kinetics (Eq. 1) [37]:

$$\ln C_t = -kt + \ln C_0, \quad (1)$$

where C_0 is the initial dye concentration, C_t is the degraded concentration, t is the degradation time, and k is the apparent first-order rate constant [38]. The kinetic plots of the photodegradation profile for different catalyst samples are depicted in Fig. 5b, and it can be observed that the rate constant of sample CNR-2 is 0.0175 min^{-1}, which is significantly higher than those of the other samples. We have further studied the stability and reusability of the as-prepared CNR-2 photocatalyst by collecting and reusing the photocatalyst for six cycles, and the results are shown in Fig. 5c. Only insignificant loss of the photocatalytic performance is observed, which might be partly caused by the loss of the photocatalysts during collection and rinsing steps, suggesting that sample CNR-2 possesses excellent repeatability.

Radical-trapping experiments were conducted with sample CNR-2 to identify the major active species in the photodegrading MO, and the results are shown in Fig. 5d. After irradiation for 60 min, with the use of 1 mM of $NaHCO_3$, the original MO concentration changed slightly, indicating that photogenerated holes are the dominant oxidizing species in the photocatalytic reaction with this ternary hybrid system. In the presence of IPA, the MO degradation changed drastically, which may be attributed to the partial hole reaction with MO directly rather than reacting with H_2O to produce ·OH radicals [39]. We can therefore conclude that the role of ·OH radicals is negligible in this photocatalysis process. In addition, the MO degradation also changed gently in the presence of BQ, suggesting that the $O_2^{\cdot-}$ radicals also are the primary reactive species contributing to the degradation of MO.

Transient photocurrent response has been regarded as a reliable criterion to evaluate the separation efficiency of the photogenerated electrons and holes [40]. As displayed in Fig. 6a, it can be seen that the as-obtained sample CNR-2 presents a higher photocurrent density than those of the binary Ag_2CO_3/Ag CNRs and CNR-0.5 samples under visible-light illumination. The remarkable photocurrent enhancement of the sample CNR-2 indicates a higher separation efficiency and a lower recombination rate of the photoinduced electron–hole pairs in such hybrid system. In addition, the EIS Nyquist plots were

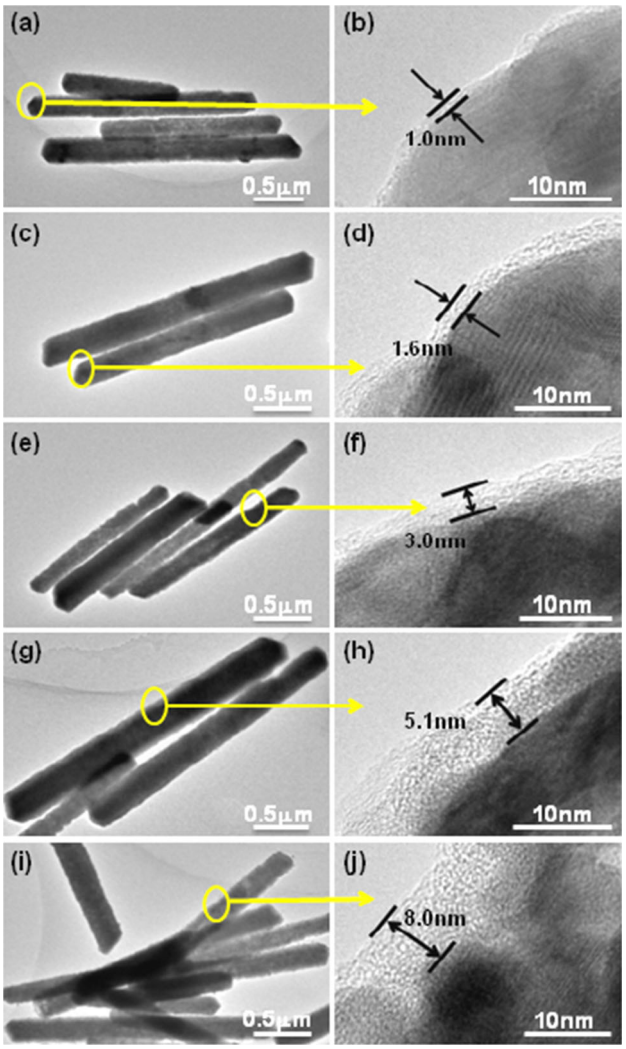

Figure 3 TEM and HRTEM images of the as-obtained 1D Ag_2CO_3/Ag/PANI ternary CNRs: **a**, **b** CNR-0.5, **c**, **d** CNR-1, **e**, **f** CNR-2, **g**, **h** CNR-3, and **i**, **j** CNR-5.

further carried out to investigate the charge transfer resistance and the carrier separation efficiency of the as-prepared samples (Fig. 6b) [41]. Compared with the binary Ag_2CO_3/Ag CNRs and CNR-0.5, the sample CNR-2 exhibits a smaller circular radius, indicating a higher electron mobility. This result is consistent with the photocurrent response analysis, which confirms that the sample CNR-2 has the ideal PANI content that balances the effect of charge separation with carrier generation to obtain optimal photoactivity.

Based on the experimental results and electronic band structures of Ag_2CO_3 and PANI, we propose a Z-scheme charge transfer model to explain the significantly improved photoactivity and photostability of the 1D ternary Ag_2CO_3/Ag/PANI hybrid system. A schematic diagram representing charge transfer process in the ternary Ag_2CO_3/Ag/PANI CNRs system is illustrated in Scheme 2. In this case, the photogenerated electrons in the valence band (VB) of Ag_2CO_3 and the highest occupied molecular orbital (HOMO) of PANI could be excited to the corresponding conduction band (CB) and the lowest unoccupied molecular orbital (LUMO) by visible-light illumination. The electrons generated in the CB of Ag_2CO_3 could not reduce O_2 to generate $O_2^{\cdot-}$ active species because the CB potential of Ag_2CO_3 (0.37 eV vs. SHE) is more positive than the reduction potential of oxygen E^{θ} ($O_2/O_2^{\cdot-}$) (–0.046 eV vs. SHE) [42]. Electrons cannot transfer directly from PANI to Ag_2CO_3 according to the traditional model in this hybrid system. The electrons in the CB of Ag_2CO_3 can migrate into the metallic Ag through the Schottky barrier, and electron transfer is faster than the electron–hole recombination process, leading to effective separation of the photogenerated carriers. On the other hand, because the Fermi energy level of metallic Ag is above the HOMO of PANI, holes in the HOMO of PANI can also flow easily into the Ag, and this process is also faster than the electron–hole recombination in PANI [43]. The metallic Ag in this Ag_2CO_3/Ag/PANI hybrid system plays a very important role in charge separation, which selectively allows the transmission of photogenerated electrons in Ag_2CO_3 and holes in PANI and leads to the neutralization of these charges. The carrier transfer process facilitated by the metal Ag NPs reduces charge recombination in respective Ag_2CO_3 and PANI, and enhances charge separation, which results in the increase of the yield of holes in Ag_2CO_3 and electrons in PANI. The photogenerated holes with strong oxidation power stay in Ag_2CO_3 and can directly oxidize dye molecule, and the electrons in PANI with strong reduction power (−1.9 eV vs. SHE) can reduce O_2 to form $O_2^{\cdot-}$ radicals [44], which promotes the degradation of dyes in the Ag_2CO_3/Ag/PANI hybrid system as what have proved in the other hybrid system reported elsewhere [45–47]. In this hybrid system, photoinduced electrons are neutralized with the aid of the metallic Ag rather than being transferred to Ag_2CO_3 to react with Ag^+ ions there [48]. As a result, the photocorrosion of Ag_2CO_3 nanorods can be inhibited, further resulting in the improved activity and stability of the Ag_2CO_3/Ag/PANI ternary CNRs.

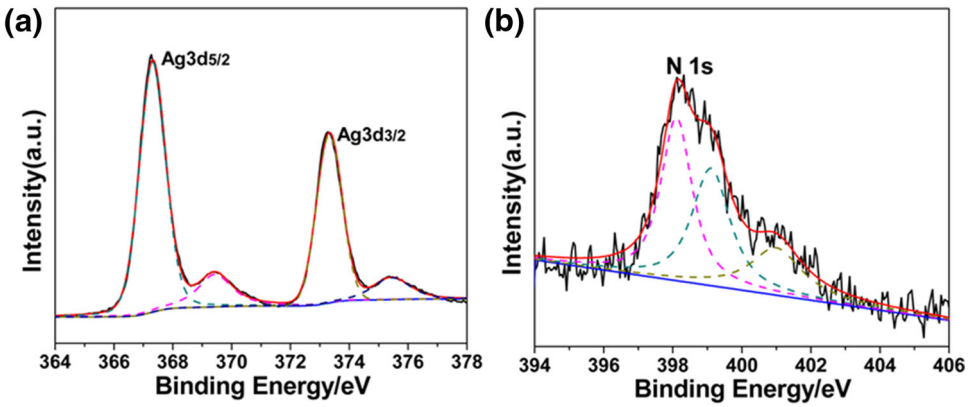

Figure 4 XPS spectra of the as-prepared sample CNR-2: **a** Ag 3d and **b** N 1s.

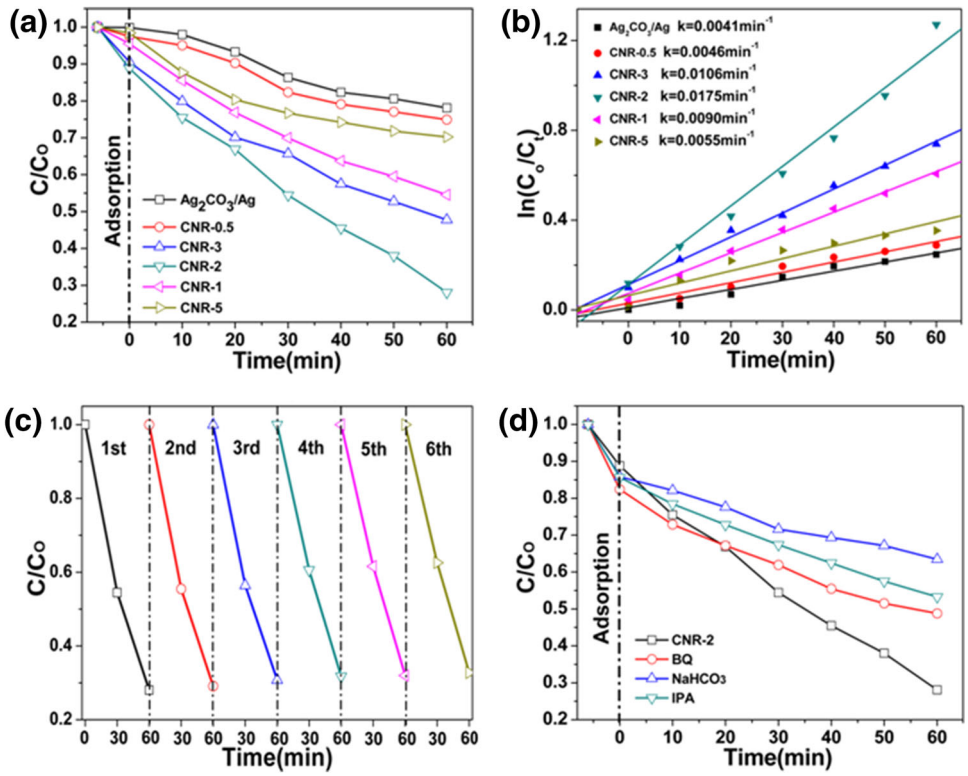

Figure 5 **a** Photocatalytic activities of the as-prepared 1D Ag_2CO_3/Ag and Ag_2CO_3/Ag/PANI CNRs for the degradation of MO under visible-light irradiation, **b** photodegradation kinetics of MO aqueous solutions over different samples, **c** cycling runs of the as-prepared sample CNR-2 for the degradation of MO, and **d** photodegradation of MO on sample CNR-2 in the presence of different scavengers under visible-light irradiation.

Conclusions

In summary, we have developed a facile route to synthesize 1D Ag_2CO_3/Ag/PANI ternary CNRs, namely a visible-light-induced reduction approach followed by simple chemisorption. Compared with Ag_2CO_3/Ag binary CNRs, the as-prepared Ag_2CO_3/Ag/PANI CNRs exhibit obviously enhanced photoelectrochemical current response and photocatalytic activity in degrading MO under visible-light illumination. It has been found that PANI modification does not affect the Ag_2CO_3/Ag structure and an optimal PANI weight percent (2.0%) is observed for the best photocatalytic performance. The enhanced visible-light-driven photocatalytic activity may be attributed to a synergistic effect between Ag_2CO_3 and PANI with Ag NPs, and a Z-scheme charge transfer model is also proposed to understand the charge separation behaviors. Due to the introduction of Ag NPs in such a ternary CNR system, the inhibition of Ag_2CO_3 photocorrosion and the effective separation of photogenerated electrons and holes can be realized, and the photostability of the products can be greatly improved. We believe that the synthetic

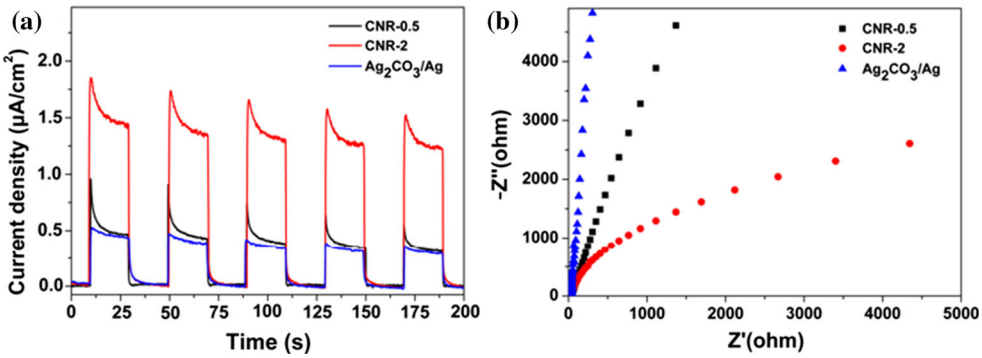

Figure 6 **a** Photocurrent response and **b** EIS Nyquist plot of the as-prepared binary Ag_2CO_3/Ag CNRs and samples CNR-0.5 and CNR-2.

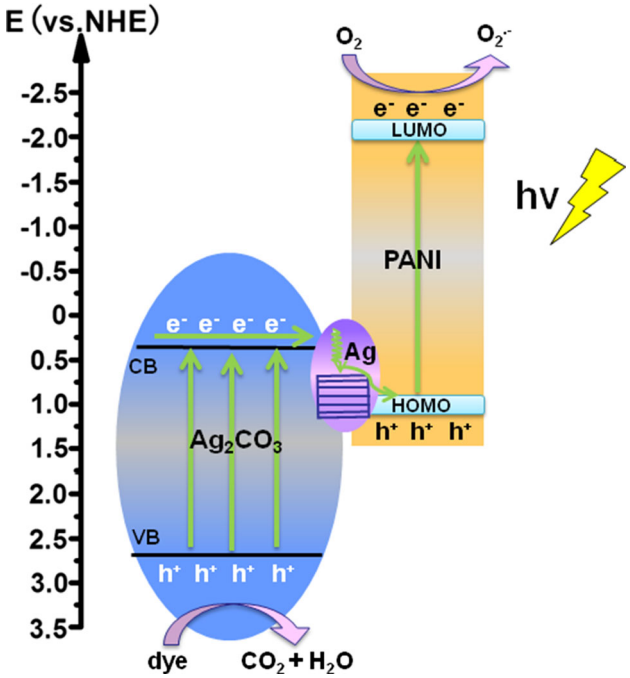

Scheme 2 Schematic diagram representing the charge transfer process in the 1D ternary Ag_2CO_3/Ag/PANI CNRs.

method presented in this work provides important insights into the design of highly efficient 1D heterostructured photocatalysts for practical environment remediation.

Acknowledgements

Financial support from the Natural Science Foundation of China (21671173, 61674166, 11504299), the Zhejiang Provincial Natural Science Foundation of China (LR14B010001), the Zhejiang Provincial Public Welfare Project (2016C31015), and the State Key Laboratory of Silicon Materials at Zhejiang University (2015-10) is gratefully acknowledged. J.Q.N. acknowledges the financial support from The Hundred Talents Program of Chinese Academy of Sciences, and Z.Y.Z. acknowledges the financial support from The Thousand Youth Talents Plan. And C.C.Z. acknowledges the partial support of an open project from State Key Laboratory of Functional Materials for Informatics, Shanghai Institute of Microsystem and Information Technology.

References

[1] Yu CL, Li G, Kumar S, Yang K, Lin RC (2014) Phase transformation synthesis of novel Ag_2O/Ag_2CO_3 heterostructures with high visible light efficiency in photocatalytic degradation of pollutants. Adv Mater 26:892–898

[2] Li JJ, Yu CY, Zheng CC, Etogo A, Xie YL, Zhong YJ, Hu Y (2015) Facile formation of Ag_2WO_4/AgX (X = Cl, Br, I) hybrid nanorods with enhanced visible-light-driven photoelectrochemical properties. Mater Res Bull 61:315–320

[3] Qiao R, Mao MM, Hu EL, Zhong YJ, Ning JQ, Hu Y (2015) Facile formation of mesoporous $BiVO_4$/Ag/AgCl heterostructured microspheres with enhanced visible-light photoactivity. Inorg Chem 54:9033–9039

[4] Gao XH, Wu HB, Zheng LX, Zhong YJ, Hu Y, Lou XW (2014) Formation of mesoporous heterostructured $BiVO_4$/Bi_2S_3 hollow discoids with enhanced photoactivity. Angew Chem Int Ed 53:5917–5921

[5] Beltran-Huarac J, Resto O, Carpena-Nuñez J, Jadwisienczak WM, Fonseca LF, Weiner BR, Morell G (2014) Single-crystal γ-MnS nanowires conformally coated with carbon. ACS Appl Mater Interfaces 6:1180–1186

[6] Deng F, Min LJ, Luo XB, Wu SL, Luo SL (2013) Visible-light photocatalytic degradation performances and thermal stability due to the synergetic effect of TiO_2 with conductive copolymers of polyaniline and polypyrrole. Nanoscale 5:8703–8710

[7] Zhang ZJ, Zheng TT, Xu JY, Zeng HB (2016) Polythiophene/Bi_2MoO_6: a novel conjugated polymer/nanocrystal hybrid composite for photocatalysis. J Mater Sci 51:3846–3853. doi:10.1007/s10853-015-9703-8

[8] Zhao ZY, Zhou Y, Wang F, Zhang KH, Yu S, Cao K (2015) Polyaniline-decorated 001 facets of $Bi_2O_2CO_3$ nanosheets: in situ oxygen vacancy formation and enhanced visible light photocatalytic activity. ACS Appl Mater Interfaces 7:730–737

[9] Kushwaha HS, Thomas P, Vaish R (2015) Polyaniline/$CaCu_3Ti_4O_{12}$ nanofiber composite with a synergistic effect on visible light photocatalysis. RSC Adv 5:87241–87250

[10] Zhang ZJ, Wang WZ, Gao EP (2014) Polypyrrole/Bi_2WO_6 composite with high charge separation efficiency and enhanced photocatalytic activity. J Mater Sci 49:7325–7332. doi:10.1007/s10853-014-8445-3

[11] Liu FW, Liu Z, Gu YH, Chen Z, Fang PF (2013) Synthesis and characterization of a conducting polyaniline/TiO_2–SiO_2 composites. J Appl Polym Sci 130:2288–2295

[12] Zhang H, Zhu YF (2010) Significant visible photoactivity and antiphotocorrosion performance of CdS photocatalysts after monolayer polyaniline hybridization. J Phys Chem C 114:5822–5826

[13] Li XY, Wang DS, Cheng GX, Luo QZ, An J, Wang YH (2008) Preparation of polyaniline-modified TiO_2 nanoparticles and their photocatalytic activity under visible light illumination. Appl Catal B 81:267–273

[14] Shang M, Wang WZ, Sun SM, Ren J, Zhou L, Zhang L (2009) Efficient visible light-induced photocatalytic degradation of contaminant by spindle-like PANI/$BiVO_4$. J Phys Chem C 113:20228–20233

[15] Zhang H, Zong RL, Zhu YF (2009) Photocorrosion inhibition and photoactivity enhancement for zinc oxide via hybridization with monolayer polyaniline. J Phys Chem C 113:4605–4611

[16] Zhu MS, Chen PL, Liu MH (2012) Ag/AgBr/graphene oxide nanocomposite synthesized via oil/water and water/oil microemulsions: a comparison of sunlight energized plasmonic photocatalytic activity. Langmuir 28:3385–3390

[17] Luo GQ, Jiang XJ, Li MJ, Shen Q, Zhang LM, Yu HG (2013) Facile fabrication and enhanced photocatalytic performance of Ag/AgCl/rGO heterostructure photocatalyst. ACS Appl Mater Interfaces 5:2161–2168

[18] Liang YH, Wang H, Liu L, Wu PF, Cui WQ, McEvoy JG, Zhang ZS (2015) Microwave-assisted synthesis of a superfine Ag/AgI photocatalyst with high activity and excellent durability. J Mater Sci 50:6935–6946. doi:10.1007/s10853-015-9245-0

[19] Yang SY, Zhang SS, Wang HJ, Yu H, Fang YP, Peng F (2015) Controlled preparation of Ag–Cu_2O nanocorncobs and their enhanced photocatalytic activity under visible light. Mater Res Bull 70:296–302

[20] Bouzid H, Faisal M, Harraz FA, Sayari SA, Ismail AA (2015) Synthesis of mesoporous Ag/ZnO nanocrystals with enhanced photocatalytic activity. Catal Today 252:20–26

[21] Zhang ZC, Li JL (2011) Ag/GaP nanoparticles with photooxidation property under visible light. J Mater Sci 46:3590–3596. doi:10.1007/s10853-011-5274-5

[22] Yang WL, Zhang L, Hu Y, Zhong YJ, Wu HB, Lou XW (2012) Microwave-assisted synthesis of porous Ag_2S–Ag hybrid nanotubes with high visible-light photocatalytic activity. Angew Chem Int Ed 51:11501–11504

[23] Wang YR, Yang WL, Zhang L, Hu Y, Lou XW (2013) Formation of MS–Ag and MS (M = Pb, Cd, Zn) nanotubes via microwave-assisted cation exchange and their enhanced photocatalytic activities. Nanoscale 5:10864–10867

[24] Li JJ, Xie YL, Zhong YJ, Hu Y (2015) Facile synthesis of Z-scheme Ag_2CO_3/Ag/AgBr ternary heterostructured nanorods with improved photostability and photoactivity. J Mater Chem A 3:5474–5481

[25] Zhang QL, Wang WJ, Li JL, Zhu JJ, Wang LJ, Zhu MF, Jiang W (2013) Preparation and thermoelectric properties of multi-walled carbon nanotube/polyaniline hybrid nanocomposites. J Mater Chem A 1:12109–12114

[26] Li TT, He YM, Lin HJ, Cai J, Dong LZ, Wang XX, Luo MF, Zhao LH, Yi XD, Weng WZ (2013) Synthesis, characterization and photocatalytic activity of visible-light plasmonic photocatalyst AgBr–$SmVO_4$. Appl Catal B 138–139:95–103

[27] Liang YH, Lin SL, Liu L, Hu JS, Cui WQ (2014) An oil-in-water self-assembly synthesis, characterization and photocatalytic properties of nano Ag@AgCl surface-sensitized $K_2Ti_4O_9$. Mater Res Bull 60:382–390

[28] Hou JG, Cao R, Jiao SQ, Zhu HM, Kumar RV (2011) PANI/$Bi_{12}TiO_{20}$ complex architectures: controllable synthesis and enhanced visible-light photocatalytic activities. Appl Catal B 104:399–406

[29] Shi L, Liang L, Wang FX, Liu MS, Sun JM (2015) Enhanced visible-light photocatalytic activity and stability over g-C_3N_4/Ag_2CO_3 composites. J Mater Sci 50:1718–1727. doi:10.1007/s10853-014-8733-y

[30] Boomi P, Prabu HG, Manisankar P, Ravikumar S (2014) Study on antibacterial activity of chemically synthesized PANI–Ag–Au nanocomposite. Appl Surf Sci 300:66–72

[31] Sen T, Shimpi NG, Mishra S, Sharma R (2014) Polyaniline/Fe_2O_3 nanocomposite for room temperature LPG sensing. Sens Act B 190:120–126

[32] Wang HH, Zhu EW, Yang JZ, Zhou PP, Sun DP, Tang WH (2012) Bacterial cellulose nanofiber-supported polyaniline nanocomposites with flake-shaped morphology as supercapacitor electrodes. J Phys Chem C 116:13013–13019

[33] Yao TJ, Shi L, Wang H, Wang FX, Wu J, Zhang X, Sun JM, Cui TY (2016) A simple method for the preparation of TiO_2/Ag–AgCl@Polypyrrole composite and its enhanced visible-light photocatalytic activity. Chem Asian J 11:141–147

[34] Dai GP, Li SY, Liu SQ, Liang Y, Zhao H (2015) Improved photocatalytic activity and stability of nano-sized Ag/Ag_2CO_3 plasmonic photocatalyst by surface modification of Fe(III) nanocluster. J Chin Chem Soc 62:944–950

[35] Liu PB, Huang Y, Yang YW, Yan J, Zhang X (2016) Sandwich structures of graphene@Fe_3O_4@PANI decorated with TiO_2 nanosheets for enhanced electromagnetic wave absorption properties. J Alloys Compd 662:63–68

[36] Zhao ZY, Zhou Y, Wang F, Zhang KH, Yu S, Cao K (2015) Polyaniline-decorated 001 facets of $Bi_2O_2CO_3$ nanosheets: in situ oxygen vacancy formation and enhanced visible light photocatalytic activity. ACS Appl Mater Interfaces 7:730–737

[37] Li CJ, Wang SP, Wang T, Wei YJ, Zhang P, Gong JL (2014) Monoclinic porous $BiVO_4$ networks decorated by discrete g-C_3N_4 nano-islands with tunable coverage for highly efficient photocatalysis. Small 10:2783–2790

[38] Luo J, Zhou XS, Zhang JQ, Du ZH (2015) Fabrication and characterization of Ag_2CO_3/SnS_2 composites with enhanced visible-light photocatalytic activity for the degradation of organic pollutants. RSC Adv 5:86705–86712

[39] Etogo A, Hu EL, Zhou CM, Zhong YJ, Hu Y, Hong ZL (2015) Facile fabrication of mesoporous $BiOCl/(BiO)_2CO_3/Bi_2O_3$ ternary flower-like heterostructured microspheres with high visible-light-driven photoactivity. J Mater Chem A 3:22413–22420

[40] Wang SL, Li JJ, Zhou XD, Zheng CC, Ning JQ, Zhong YJ, Hu Y (2014) Facile preparation of 2D sandwich-like CdS nanoparticles/nitrogen-doped reduced grapheme oxide hybrid nanosheets with enhanced photoelectrochemical properties. J Mater Chem A 2:19815–19821

[41] Etogo A, Liu R, Ren JB, Qi LW, Zheng CC, Ning JQ, Zhong YJ, Hu Y (2016) Facile one-pot solvothermal preparation of Mo-doped Bi_2WO_6 biscuit-like microstructures for visible-light-driven photocatalytic water oxidation. J Mater Chem A 4:13242–13250

[42] Song SQ, Cheng B, Wu NS, Meng AY, Cao SW, Yu JG (2016) Structure effect of graphene on the photocatalytic performance of plasmonic Ag/Ag_2CO_3–rGO for photocatalytic elimination of pollutants. Appl Catal B 181:71–78

[43] Wang QZ, Hui J, Li JJ, Cai YX, Yin SQ, Wang FP, Su BT (2013) Photodegradation of methyl orange with PANI-modified BiOCl photocatalyst under visible light irradiation. Appl Surf Sci 283:577–583

[44] Lin X, Hou J, Jiang S, Lin Z, Wang M, Che GB (2015) A Z-scheme visible-light-driven $Ag/Ag_3PO_4/Bi_2MoO_6$ photocatalyst: synthesis and enhanced photocatalytic activity. RSC Adv 5:104815–104821

[45] Li WB, Feng C, Dai SY, Yue JG, Hua FX, Hou H (2015) Fabrication of sulfur-doped g-C_3N_4/Au/CdS Z-scheme photocatalyst to improve the photocatalytic performance under visible light. Appl Catal B 168–169:465–471

[46] Chen ZH, Wang WL, Zhang ZG, Fang XM (2013) High-efficiency visible-light-driven Ag_3PO_4/AgI photocatalysts: Z-scheme photocatalytic mechanism for their enhanced photocatalytic activity. J Phys Chem C 117:19346–19352

[47] Chen ZH, Bing F, Liu Q, Zhang ZG, Fang XM (2015) Novel Z-scheme visible-light-driven Ag_3PO_4/Ag/SiC photocatalysts with enhanced photocatalytic activity. J Mater Chem A 3:4652–4658

[48] Tang JT, Liu YH, Li HZ, Tan Z, Li DT (2013) A novel Ag_3AsO_4 visible-light-responsive photocatalyst: facile synthesis and exceptional photocatalytic performance. Chem Commun 49:5498–5500